K-shell ionization by ^{16}O and ^{32}S ions: Reduced-velocity dependence of the binding effect

J. Seidel, S. Röhl,* R. Lorek, S. Huchler,† and M. Dost
Institut für Kernphysik, Universität Köln, D-5000 Köln 41, Germany
(Received 19 April 1985)

K-shell ionization probabilities P_K were measured for 2.2-MeV/u ^{16}O ions with impact parameter $b=16$—51 fm on 24 targets ranging from Sc to Bi. For Bi, the distribution $P_K(b)$ was also measured. Total K-shell ionization cross sections σ_K for ^{16}O and ^{32}S projectiles are reported for the same target range. Semiclassical calculations using the velocity-dependent electron binding energies from the relativistic two-center approximation of Andersen, Laegsgaard, and Lund reproduce both P_K and σ_K very well, except where polarization effects become important.

I. INTRODUCTION

One of the main features in collisions of heavy ions with atoms is the massive distortion of the target K-electron binding energy by the projectile charge during the collision. For very heavy systems, with a united-atom (UA) nuclear charge $Z_{UA} \geq 130$, the production of K-shell vacancies in the heavier collision partner in adiabatic central collisions was found[1] to be via direct Coulomb excitation from the $1s\,\sigma$ orbital, with nearly the united-atom K-shell binding energy. Similarly, for close collisions of heavy systems with $68 \leq Z_{UA} \leq 107$, the K-shell ionization of the lighter partner can be quantitatively understood[2] as direct excitation from the $2p\,\sigma$ orbital, with nearly the UA L-shell binding energy. These results[1,2] seem to suggest that the UA binding energy is adequate for the description of central collisions in general. It is the principal aim of the present work to study the effective K-shell binding when proceeding from adiabatic to fast, and from very asymmetric to almost symmetric, collisions.

We studied the K-shell ionization probability P_K at small impact parameter, and the total K-shell cross section σ_K for collision systems with charge ratio Z_1/Z from 0.1 to 0.8 and reduced velocity $\xi_K=(2/\Theta_K)v_1/v_K$ from 0.2 to 1.2. Here, Z_1 and v_1 are the atomic number and the velocity of the projectile, Z and v_K are the atomic number and Bohr velocity of the target, and Θ_K is the screening constant. This parameter range is covered in 2.2 MeV/u collisions of ^{16}O and ^{32}S ions with target atoms ranging from Sc through Bi.

After briefly outlining the experimental procedure in Sec. II, we describe in Sec. III the data treatment and present the results of our measurements. In Sec. IV we describe our analysis. A discussion is given in Sec. V and the conclusions are drawn in Sec. VI.

II. EXPERIMENT

Our experimental technique is essentially standard and has been described for the most part previously.[3] We derive the K-shell ionization probability from particle—x-ray coincidences, duly corrected for detection efficiency and fluorescence yield. Total cross sections are obtained from the x-ray singles intensities. We refer to Ref. 3 for additional details.

We used beams of 35-MeV $^{16}O^{5+}$ and 70-MeV $^{32}S^{9+}$ ions from the High Voltage Engineering Corporation model FN tandem accelerator at the University of Köln. Checks on charge-state effects were performed with $^{16}O^{7+}$ ions of the same velocity, incident on 1-μg/cm^2 low-Z targets. Beam intensities were limited to typically $5q$ pA (low-Z regime) and to $10q$ nA (high-Z regime) for ions of charge state q.

Scattered particles were detected by a 3-mm-deep annular parallel-plate avalanche counter (PPAC) of 10-cm diameter placed at 0°. Eight anode rings defined mean scattering angles θ from 6.5° to 23.5°. Entrance and cathode foils were made of 8-μm Mylar and 5-μm aluminized Mylar, respectively. The PPAC was operated at 550 V and with isobutane at a pressure of 11 mbar. Part of the data was taken for ions scattered into $\theta=25°$—35° with another PPAC. Two Si surface-barrier detectors at 170° and 45° served for monitoring and cross-section normalization.

The K x rays were detected at right angles to the beam by a 1140-mm^2×4-mm-thick NaI(Tl) scintillator and a 0.5-cm^3 high-purity germanium (HPGe) diode, placed behind 25-μm Mylar vacuum windows. The coincident x-ray yields were measured with the NaI(Tl) scintillator, which subtended a solid angle of 2.8 sr. The time resolution as measured against the fast (<1 ns) PPAC is shown in Fig. 1. It varies slowly from 3.5 ns at 78 keV (Bi) to 9 ns at 4.2 keV (Sc). The real- to random-coincidence-count-rate ratio was better than 3:1 in all cases. No indication of time structure in the beam was found in the 400-ns-wide time spectra.

The x-ray singles yields were measured with the high-resolution HPGe detector [172 eV full width at half maximum (FWHM) at 5.9 keV] which also served as efficiency standard and monitor for target impurities. Its efficiency was calibrated with photon sources of ^{49}V, ^{57}Co, ^{65}Zn, ^{109}Cd, ^{133}Ba, ^{152}Eu, and ^{241}Am placed at the beam-spot position.

A list of targets and their characteristics is given in Table I. In order to minimize double scattering,[4,5] thin self-supporting targets were used whenever possible. In

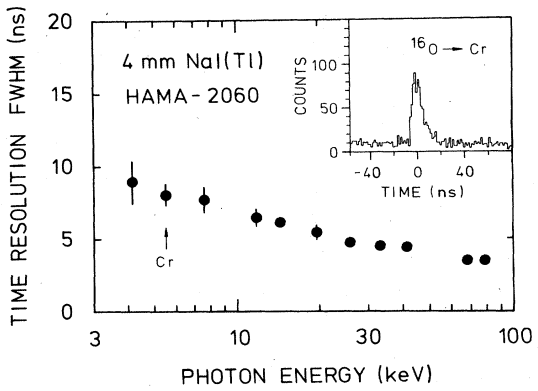

FIG. 1. Time resolution as a function of photon energy. The scintillator was coupled to a Hamamatsu 2060 photomultiplier. Inset shows part of the time spectrum obtained from ^{16}O-Cr K x-ray coincidences with a resolution of 8 ns (FWHM).

the other cases, the correction of the PPAC singles count rate for scattering off the carbon backings was determined from a C reference target. The correction remained below 5%, except for the 1-$\mu g/cm^2$ Sc and Cr targets.

Conventional fast-slow coincidence circuits were applied for signal processing. Singles count rates were scaled down to less than 1 kHz to prevent dead time of the analyzer system. Dead time was monitored using beam-current-triggered pulses fed into the preamplifiers. Data were recorded on a Digital Equipment Corporation PDP 11/70 computer in event mode on magnetic tape and analyzed off line to ensure appropriate window settings.

III. DATA REDUCTION AND RESULTS

As secondary processes contribute to some of the measured x-ray yields, we will explain the data treatment in some detail before we present our results.

For Sm, Ho, Tm, and Ta, internal K-shell conversion after nuclear Coulomb excitation contributed to coincident and singles x-ray spectra. Corresponding corrections were derived from the simultaneously measured low-energy γ transitions and the internal K-shell conversion coefficients α_K of Ref. 6. Large net errors (up to 54%) resulted in some cases for the x-ray yields from direct ionization.

The coincident x-ray yield was corrected for double-scattering events using a generalized version[5] of the correction formula given in Ref. 4. It takes proper account of the angular acceptance of the PPAC and of the tilted-target geometry. This formula does not account for

TABLE I. Target areal densities and corrections to the coincidence yields in the measurement of P_K. Given are the quantities $1-P_K/P_K^{\text{uncorr}}$, with P_K^{uncorr} being the uncorrected ionization probability. Corrections are labeled IC for internal K-shell conversion, DS for double scattering, and EL for projectile energy loss. Corrections below 3% are not listed.

Target[a]	Atomic number	Areal density ($\mu g/cm^2$)	Correction IC	DS	EL
Sc	21	22		0.28	
Ti	22	50			
Cr/C	24	16		0.13	
Fe	26	23		0.15	
Ni	28	27		0.07	
Cu	29	77		0.11	
Zn/C	30	185		0.22	
Se	34	22			
Sr/C	38	15			
Zr	40	495		0.12	−0.09
^{92}Mo	42	334		0.06	−0.06
Ru/C	44	82			
Ag	47	349		0.03	−0.06
Cd	48	344		0.03	−0.06
Sn	50	147			
Te/C	52	99			
Ba/C	56	93			
Ce/C	58	50			
Sm/C	62	13	0.62		
Ho	67	65	0.84		
Tm	69	46	0.82		
Ta	73	100	0.71		
^{196}Pt/C	78	207			
Au	79	150			
^{207}Pb	82	229			
Bi	83	93			

[a]Natural isotopic composition, unless specified otherwise; /C indicates carbon backing.

possible ionization by the recoiling target nuclei.

The measured x-ray yields for Zr, Mo, Ag, and Cd were corrected for projectile energy loss in the target. Corrections are largest for Zr, where they amount to 9% and 12% for coincident and singles yields, respectively. A summary of all corrections applied to the coincident yields is contained in Table I.

Collisional alignment of outer-shell vacancies in multiply ionized atoms might cause anisotropic K x-ray emission. However, Jitschin *et al.*[7] found the L_3-subshell alignment of heavy atoms ($Z \geq 54$) in collisions with heavy ions to be considerably smaller than predicted by semiclassical theory[8] and even much smaller than observed experimentally in light-ion-induced ionization.[9] In keeping with this result, Horsdal-Pedersen *et al.*[10] observed isotropic target K x-ray emission in collisions of 33-MeV ^{19}F ions with Ar, a case which is very similar to our low-Z situation. We therefore assume isotropic K x-ray emission for all collision systems studied here.

Furthermore, the K-shell-fluorescence yield could differ[11] from its single-vacancy value ω_K.[12] Calculations of inner-shell transition rates are available for a few selected multiple-vacancy configurations only.[13,14] Hall *et al.*,[15] on the other hand, derived the average K-fluorescence yield of Ti for various projectiles from experimental data. It was found to be 14% and 17% above the single-vacancy value for 2.2 MeV/u oxygen and chlorine collisions, respectively. A similar estimate[16] holds for ^{16}O impact on Ni. The observed changes in ω_K are comparable to our experimental uncertainties at low Z, and should vanish for heavier atoms.[17] We therefore use the single-vacancy value of ω_K at all Z.

Total ionization cross sections σ_K were determined relative to the Rutherford cross section at 45°. Figures 2 and 3 display the results for 35-MeV ^{16}O and 70-MeV ^{32}S impact. The theoretical curves in Figs. 2 and 3 are explained in Sec. IV. The cross sections vary by six orders of magnitude over the range of target elements. The uncertainties in cross-section normalization (8%) and detection efficiency (5%, except at the lowest x-ray energies) result in experimental errors of 10% on the average. Published data[15,18–21] for ^{16}O incident on thin Sc, Ti, Fe, Ni, Cu, and Ag targets and on seven thick targets, from Mo to Bi,

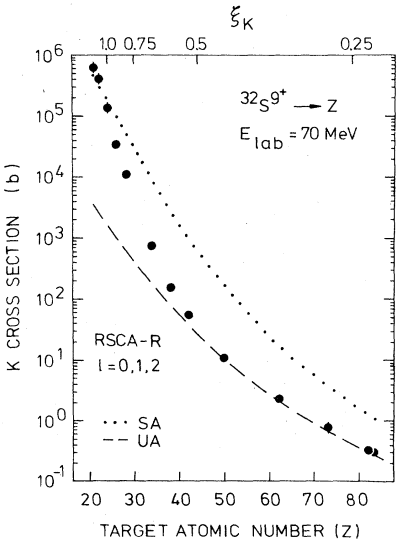

FIG. 3. Same as Fig. 2, but for 2.2-MeV/u $^{32}S^{9+}$ ions.

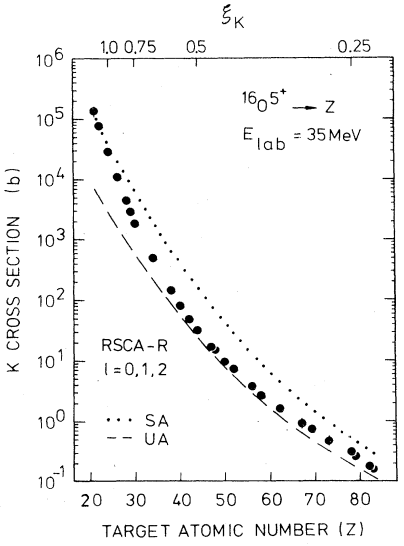

FIG. 2. Total K-shell ionization cross sections σ_K for 2.2-MeV/u $^{16}O^{5+}$ ions on targets from Sc to Bi. RSCA-R curves are explained in the text. Labels SA and UA refer to the handling of K-electron binding in the separated- and united-atom limits.

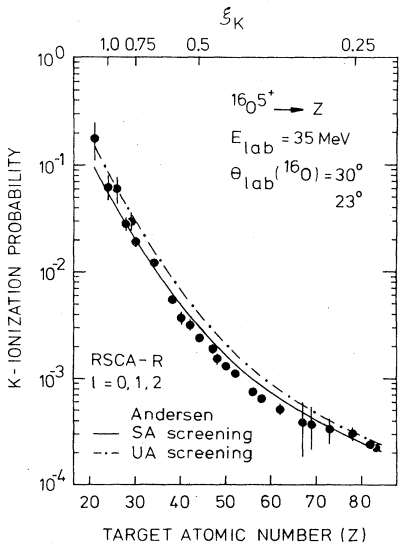

FIG. 4. Target K-shell ionization probability P_K in close collisions with 2.2-MeV/u $^{16}O^{5+}$ ions. The scattering angle 23° refers to Sc and Cr, and 30° to all heavier targets. Curves represent RSCA-R calculations. Treatment of K-electron binding in the approximation by Andersen *et al.* (Ref. 28) is explained at the end of Sec. IV.

at similar impact energies compare well with our results, as does a measurement for ^{32}S on Sn, Ref. 22.

In Fig. 4, we show the ionization probability P_K in close collisions with 35-MeV ^{16}O ions. Again, the curves are explained in Sec. IV. The impact parameters vary from $b=16\pm2$ fm for Sc to $b=51\pm9$ fm for Bi, where the uncertainties assigned to b combine[3] classical and quantum-mechanical[23] uncertainties. Figure 5 gives the impact-parameter dependence of P_K for 35-MeV ^{16}O incident on Bi. The experimental error for P_K is about 10% on the average and is dominated by the detection efficiency and the statistics of the real-coincidence yield. In some cases, the corrections listed in Table I also contribute significantly to the net error. A few isolated values of P_K with ^{16}O ions of similar energy are available in the literature. The values[24–26] for Ni and Cu agree with our results. The values[26] for Zr and Ag at $\theta=90°$ are almost a factor of 2 above the present results. The measured angular distribution[26] of P_K for Zr and Ag is nearly isotropic and does therefore not account for the discrepancy.

The results for P_K and σ_K for Sc and Cr, measured with the 1-μg/cm^2 targets and charge states $q=5+$ and $7+$, are compared in Table II with those obtained with thicker targets. The results for P_K agree within error bars. We therefore conclude that the double-scattering correction in P_K was properly done, that ionization by recoiling nuclei is negligible, and that no measurable contribution by electron capture is present in P_K. In contrast, the σ_K for $q=7+$ and for the average $\langle q\rangle$ are about 50% higher than for $q=5+$. This charge-state effect agrees well with the findings of Hall *et al.*[15] for ^{16}O incident on Ti. Tables III and IV provide a summary in numerical form of the data displayed in Figs. 2–5.

IV. ANALYSIS

In this section we compare the experimental data to calculations carried out in the framework of the relativistic semiclassical approximation (RSCA) as formulated by Rösel *et al.*[27] In these calculations, one-center Dirac wave functions describe the K electrons, and the projectile is assumed to move along the classical Coulomb trajectory. Nuclear recoil is included in the evaluation of the radial form factor, which method we indicate by RSCA-R.

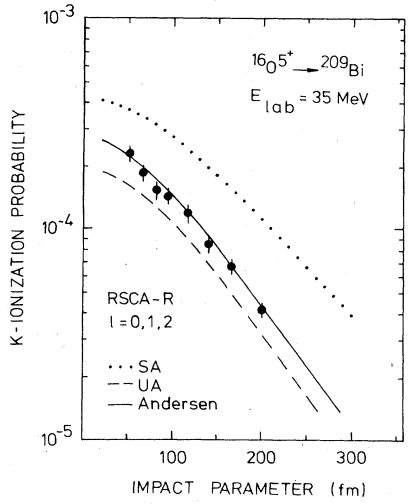

FIG. 5. K-shell ionization probability for 2.2-MeV/u $^{16}O^{5+}$ ions incident on Bi. The adiabatic radius of this collision is 150 fm. Three different treatments of K-electron binding energy combined with the RSCA-R method are compared; corresponding curves are labeled as in Figs. 2–4.

Electron final states are considered up to angular momentum $l=2$, since monopole ($l=0$) plus dipole ($l=1$) ionization alone represent more than 98% of the calculated cross sections. The large variation of P_K and σ_K with target Z is on the whole reproduced by RSCA using the separated-atom (SA) or UA K-electron binding, as illustrated by the dotted and dashed curves in Figs. 2 and 3. Quantitative agreement, however, is not obtained with either one of these limiting assumptions. The data show a smooth transition from the SA limit at large ξ_K to the UA limit at small ξ_K.

The important modifications of σ_K and P_K resulting from the transient change in electron binding energy and momentum distribution by the presence of the projectile charge Z_1e must therefore be treated in more detail. For this purpose, we have evaluated the relativistic approximation given by Andersen *et al.*[28] In this approximation, the time-dependent $1s\,\sigma$ binding is replaced by an effective two-center binding energy E_B, whereas the radial

TABLE II. Results on P_K and σ_K obtained with 2.2-MeV/u $^{16}O^{5+}$ and $^{16}O^{7+}$ ions, and 1-μg/cm^2 targets of Sc and Cr. For comparison, the "thick"-target values shown in Figs. 2 and 4 are added; $\langle q\rangle$ is the equilibrium charge state. The uncertainty of x-ray-detection efficiency is not contained in the quoted errors. Numbers in parentheses give power of 10; e.g., $1.9\pm0.19(-1)=(1.9\pm0.19)\times10^{-1}$.

Target	Areal density (μg/cm^2)	Charge state	$P_K(\theta=23°)$	σ_K (b)
Sc	1	5+	1.9±0.19(−1)	8.85±0.65(+4)
	1	7+	2.2±0.21(−1)	1.33±0.10(+5)
	22	$\langle q\rangle$	1.8±0.40(−1)	1.35±0.14(+5)
Cr	1	5+	6.8±0.66(−2)	1.91±0.15(+4)
	1	7+	6.9±0.68(−2)	2.73±0.21(+4)
	16	$\langle q\rangle$	6.3±1.20(−2)	2.90±0.21(+4)

TABLE III. Summary of the results with 35-MeV $^{16}O^{5+}$ beam displayed in Figs. 2, 4, and 5. Numbers in parentheses give power of 10; e.g., $1.8\pm0.67(-1)=(1.8\pm0.67)\times10^{-1}$.

Target	Atomic number	ξ_K	θ (deg)	b (fm)	$P_K(\theta)$	σ_K (b)
Sc	21	1.17	23.5	16±2	1.8±0.67(−1)	1.4±0.27(+5)
Ti	22	1.11				7.7±1.20(+4)
Cr	24	1.01	23.5	19±2	6.3±1.55(−2)	2.9±0.35(+4)
Fe	26	0.92	30	16±3	6.0±1.66(−2)	1.1±0.11(+4)
Ni	28	0.85	30	17±3	2.8±0.31(−2)	4.6±0.45(+3)
Cu	29	0.81	30	18±4	3.0±0.58(−2)	2.9±0.30(+3)
Zn	30	0.78	30	18±4	1.9±0.24(−2)	1.8±0.18(+3)
Se	34	0.68	30	21±4	1.2±0.12(−2)	5.1±0.51(+2)
Sr	38	0.60	30	23±4	5.4±0.54(−3)	1.5±0.15(+2)
Zr	40	0.56	30	25±5	3.8±0.60(−3)	8.1±1.20(+1)
Mo	42	0.53	30	26±5	3.4±0.43(−3)	4.9±0.60(+1)
Ru	44	0.50	30	27±5	2.4±0.24(−3)	3.2±0.32(+1)
Ag	47	0.47	30	29±5	1.9±0.22(−3)	1.7±0.17(+1)
Cd	48	0.45	30	29±5	1.5±0.20(−3)	1.6±0.19(+1)
Sn	50	0.43	30	31±6	1.3±0.13(−3)	9.5±0.95(+0)
Te	52	0.41	30	32±6	1.1±0.10(−3)	7.3±0.73(+0)
Ba	56	0.38	30	34±6	7.5±0.71(−4)	3.8±0.38(+0)
Ce	58	0.36	30	36±7	6.6±0.64(−4)	2.7±0.30(+0)
Sm	62	0.34	30	38±7	5.2±0.63(−4)	1.7±0.17(+0)
Ho	67	0.31	30	41±7	3.9±2.10(−4)	9.3±1.30(−1)
Tm	69	0.29	30	42±8	3.7±1.60(−4)	7.3±1.00(−1)
Ta	73	0.27	30	45±8	3.3±0.92(−4)	4.9±0.71(−1)
Pt	78	0.25	30	48±9	3.0±0.41(−4)	3.3±0.35(−1)
Au	79	0.25				2.6±0.29(−1)
Pb	82	0.24	30	50±9	2.4±0.22(−4)	1.8±0.18(−1)
Bi	83	0.23	30	51±9	2.3±0.21(−4)	1.6±0.16(−1)
			23.5	66±6	1.9±0.18(−4)	
			19.6	79±7	1.5±0.15(−4)	
			16.4	95±9	1.4±0.14(−4)	
			13.5	115±11	1.2±0.12(−4)	
			11.1	141±13	8.4±0.84(−5)	
			9.3	168±15	6.8±0.68(−5)	
			7.8	200±16	4.1±0.41(−5)	

form factor is calculated for a "relaxed" Dirac atom of modified size, parametrized by an effective atomic number Z'. The effective values E_B and Z' are obtained by varying Z' so as to maximize the approximate two-center binding energy[28]

$$E_B(d,Z_1,Z')=(1-\gamma')mc^2-(Z'-Z_s)e^2/\gamma' r'_K + \Delta E_B(d,Z_1,Z')-\Delta E_{\text{screen}} \quad (1)$$

for a characteristic internuclear distance d, fixed before variation. Here, m is the electron mass, $Z_s=Z-0.3$ is the screened-target atomic number, and $\gamma'=(1-\alpha^2Z'^2)^{1/2}$, where α is the fine-structure constant. The radius $r'_K=a_0/Z'$ characterizes the radial extension of the relaxed nonrelativistic K shell; a_0 is the Bohr radius of hydrogen. The term $\Delta E_B(d,Z_1,Z')$ represents the additional binding energy of the electron and the projectile charge at the velocity- and impact-parameter-dependent distance d from the target nucleus. This dis-

TABLE IV. Ionization cross sections σ_K measured with 70-MeV $^{32}S^{9+}$ beam displayed in Fig. 3. Notation same as for Table III.

Target	Atomic number	ξ_K	σ_K (b)
Sc	21	1.17	6.4±1.35(+5)
Ti	22	1.11	4.0±0.63(+5)
Cr	24	1.01	1.4±0.19(+5)
Fe	26	0.92	3.6±0.46(+4)
Ni	28	0.85	1.1±0.12(+4)
Se	34	0.68	7.4±0.81(+2)
Sr	38	0.60	1.6±0.16(+2)
Mo	42	0.53	5.5±0.60(+1)
Sn	50	0.43	1.1±0.12(+1)
Sm	62	0.34	2.4±0.28(+0)
Ta	73	0.27	8.3±1.90(−1)
Pb	82	0.24	3.4±0.41(−1)
Bi	83	0.23	3.2±0.33(−1)

tance is chosen according to the plausible estimate[28]

$$d=[d_{\min}^2(b)+r_{\mathrm{ad}}^2]^{1/2}\ , \tag{2}$$

where $d_{\min}(b)$ is the minimum internuclear distance on a trajectory with impact parameter b, and $r_{\mathrm{ad}}=\xi_K r_K$ is the adiabatic radius[29] of the collision. Finally, $\Delta E_{\mathrm{screen}}$ corrects for screening by the outer electrons.

This modified binding energy $E_B(d,Z_1,Z')$ is then used in the RSCA-R calculation[27] together with a bound-state Dirac wave function for atomic number Z'. While for $P_K(b)$, the impact parameter b, at a given ξ_K, fixes at the same time the value of E_B, the calculation of σ_K requires integration over $P_K(b)$, each one with a b-dependent value of E_B. We have avoided this procedure by evaluating Eq. (1) for the representative internuclear distance $\langle d\rangle=r_{\mathrm{ad}}$. We have then used the resulting b-independent values E_B and Z' in the calculation of the σ_K.

As a quantitative measure of the binding effect on σ_K and P_K, we introduce the reduced cross-section ratio

$$R_\sigma(Z_1)=\sigma_K(Z_1)/Z_1^2\sigma_K^{\mathrm{RSCA}}(^2_1\mathrm{H})\ , \tag{3}$$

and, analogously, the reduced probability ratio

$$R_P(Z_1,b)=P_K(Z_1,b)/Z_1^2P_K^{\mathrm{RSCA}}(^2_1\mathrm{H},b)\ , \tag{4}$$

both displayed in Fig. 6. These ratios measure the deviation of σ_K and P_K from Z_1^2 scaling ($R_\sigma=R_P=1$), valid for unmodified binding. We chose ionization by deuterons ($^2_1$H) rather than protons of 2.2 MeV/u for reference, as they represent practically unmodified binding and have a Z/A equal to that of ^{16}O and ^{32}S. The $^2_1$H cross sections are calculated in RSCA-R.

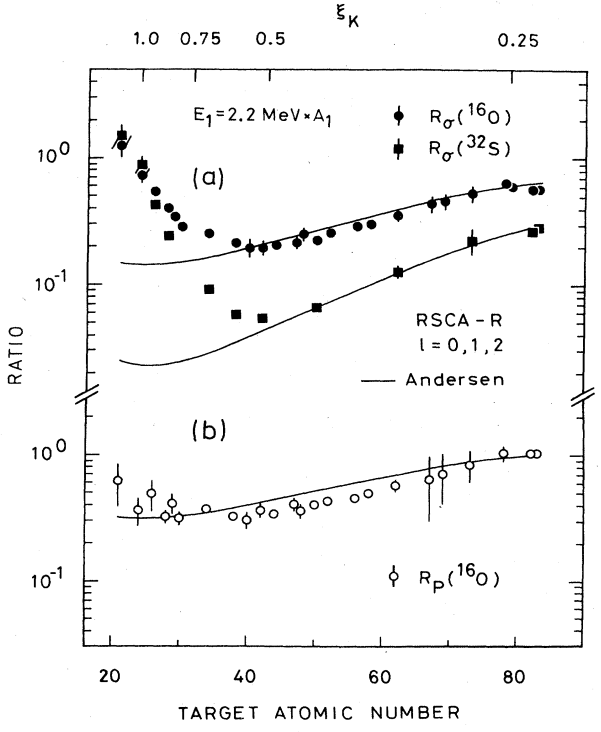

FIG. 6. (a) Ratios R_σ of reduced cross sections, as defined by Eq. (3), for ^{16}O and ^{32}S projectiles of 2.2 MeV/u. (b) Ratios R_P, as defined by Eq. (4), for ^{16}O ions of impact parameter between 16 and 51 fm. Labeling of RSCA-R curves is the same as in Figs. 4 and 5.

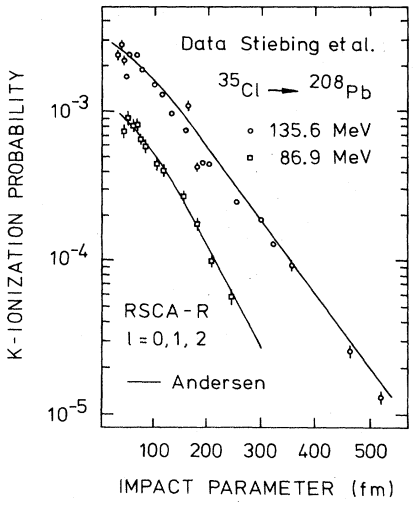

FIG. 7. Results of Stiebing *et al.* (Ref. 30) on $P_K(b)$ for ^{35}Cl ions of 2.5 and 3.9 MeV/u impinging on Pb. Data are compared to RSCA-R calculations using the relativistic binding approximation of Andersen *et al.* (Ref. 28) as explained in Sec. IV.

Limiting ourselves to the probabilities P_K, we show the comparison of measured absolute values with those obtained by RSCA-R calculations, using Eq. (1) for E_B, in Figs. 4, 5, and 7. In addition to our own data, we also analyzed the $P_K(b)$ results of Stiebing *et al.*[30] for ^{35}Cl ions of 86.9 and 135.6 MeV incident on Pb (Fig. 7). The agreement of the calculated P_K in ^{16}O- and ^{35}Cl-induced collisions with experiment is very satisfactory, as the solid curves in Figs. 4, 5, and 7 clearly show. This, in particular, improves considerably on the earlier UA analysis of the ^{35}Cl data.[30]

For completeness, we mention the relatively minor point of the outer screening correction $\Delta E_{\mathrm{screen}}$ in Eq. (1). Andersen *et al.*[28] evaluated this correction for the united atom. However, even in a collision that is adiabatic for the K shell, the outer electrons may adjust more slowly to the modified nuclear charge, and SA screening may become more realistic. We therefore simply left it to an empirical comparison to determine whether separated-atom or united-atom screening in the evaluation of Eq. (1) came closer to the data. Both versions are displayed in Fig. 4, while elsewhere we have retained only the slightly superior SA screening.

V. DISCUSSION

The ratio R_σ shown in Fig. 6 reaches the lowest values of 0.20 and 0.06 as compared to unity, which illustrates the importance of the binding effect. A very similar behavior is found for the $R_P(^{16}\mathrm{O})$ of Fig. 6, which has a minimum value of 0.30. The observed tendency towards

increased ionization probability and cross section for the nonadiabatic and more-symmetric collisions near $\xi_K = 1$ overrides the expected further decrease of R_P and R_σ with increasing charge ratio Z_1/Z. This may be attributed[16] to the polarization of the electron wave function which was observed earlier[3,16] in P_K as well as σ_K whenever Z_1/Z was sufficiently large and the collision dominated by an effective internuclear distance $d \simeq r_K$. The approximation by Andersen *et al.*[28] does not include polarization and may therefore not be compared to the data in the region $\xi_K > 0.5$.

For $\xi_K < 0.5$, the RSCA-R curves employing this approximation to describe the effective binding reproduce $R_\sigma(^{16}\text{O})$, $R_\sigma(^{32}\text{S})$, and $R_P(^{16}\text{O})$ very satisfactorily. The underlying two-center picture of direct Coulomb ionization and its approximate evaluation are thus shown to be correct. In the same data range, RSCA-R calculations using the nonrelativistic two-center formula, also elaborated by Andersen *et al.*,[25,28] failed to reproduce the experimental P_K and σ_K by factors between 1.3 and 1.7, as expected for collisions involving K electrons in heavy atoms.

The choice made in Eq. (2) for the internuclear distance d at which $E_B(d,Z_1,Z')$ is to be evaluated implies a combination of the trajectory geometry [entering via $d_{\min}(b)$] and the adiabaticity or relative velocity of the collision (entering via $r_{\text{ad}} = \xi_K r_K$). In close collisions, with $b \ll r_K$, say, one generally also has $d^2_{\min} \ll (\xi_K r_K)^2 = r^2_{\text{ad}}$ and therefore $d \simeq r_{\text{ad}}$. For example, our data range from Sc to Bi covers, for ^{16}O collisions, an interval $b = 16$–51 fm while r_{ad} varies from 3000 to 150 fm, yielding effective internuclear distances $d = 3000$–170 fm. The effective binding energy in close collisions is thus expected to be $E_B(r_{\text{ad}},Z_1,Z')$. This is, in fact, confirmed by the comparison of the experimental $R_P(^{16}\text{O})$ with the corresponding RSCA-R curve for $\xi_K < 0.5$ in Fig. 6, which shows good agreement.

The plausible simplifying choice $\langle d \rangle = r_{\text{ad}}$, used in calculating σ_K in RSCA-R, results in the identical effective binding energy $E_B(r_{\text{ad}},Z_1,Z')$ for the collisions contributing to σ_K. The very good agreement, for $\xi_K < 0.5$, of $R_\sigma(^{16}\text{O})$ and $R_\sigma(^{32}\text{S})$ with the RSCA-R prediction implies therefore that whenever $d^2_{\min} \ll r^2_{\text{ad}}$, the internuclear distance contributing most significantly to P_K and to σ_K is nearly the same. In particular, central collisions are not generally described best by using the united-atom binding energy; this only works when the collision is very adiabatic so that $d \ll r_K$. In the latter case, the best σ_K is also obtained by using the UA binding energy.

VI. CONCLUSION

The preceding discussion of K-shell ionization by heavy ions has shown that for a large variety of collision systems the process can be described in detail as direct Coulomb excitation into the continuum, in the same terms as for light-ion–atom collisions. It is found that an effective internuclear distance can be defined at which one must evaluate the two-center electron binding energy that is to be used in the calculation of Coulomb ionization. For a wide range of collision systems, this effective internuclear distance is governed by the relative projectile velocity alone and is quite independent of impact parameter. Even in central collisions, the adequate electron binding energy in the presence of a heavy projectile is usually different from the united-atom value, except in extremely adiabatic collisions.

The recently developed coupled-channels method,[31] which treats electron excitations in collisions of ions with complex atoms, holds every promise of putting the successful approximation of Andersen *et al.*[28] on a more general basis, and to make the use of such quantities as effective distance and binding energy unnecessary. Moreover, we expect that the coupled-channels calculations will account, on the same general basis, for the polarization effects mentioned earlier.

ACKNOWLEDGMENTS

This work was supported by Deutsche Forschungsgemeinschaft and by Bundesministerium für Forschung und Technologie, Bonn, Germany. We are particularly indebted to F. Rösel and D. Trautmann who provided us with the current version of their RSCA computer code. The computing assistance of M. Neschen and the help of E. Abeln in part of the data taking are gratefully acknowledged.

---

*Present address: Siemens AG, München, Germany.

†Present address: Technische Universität München, Garching, Germany.

[1]F. Bosch, D. Liesen, P. Armbruster, D. Maor, P. H. Mokler, H. Schmidt-Böcking, and R. Schuch, Z. Phys. A **296**, 11 (1980); P. Armbruster, in *Quantum Electrodynamics of Strong Fields,* edited by W. Greiner (Plenum, New York, 1983), p. 179.

[2]D. Maor, D. Liesen, P. H. Mokler, B. Rosner, H. Schmidt-Böcking, and R. Schuch, Phys. Rev. A **27**, 2881 (1983).

[3]M. Dost, S. Hoppenau, J. Kising, S. Röhl, and P. Schorn, Phys. Rev. A **24**, 693 (1981).

[4]M. Dost, Nucl. Instrum. Methods **169**, 305 (1980).

[5]E. Friederichs, Diplomarbeit (Masters thesis), University of Köln, 1980.

[6]*Table of Isotopes,* 7th ed., edited by C. M. Lederer and V. S. Shirley (Wiley Interscience, New York, 1978).

[7]W. Jitschin, R. Hippler, R. Shanker, H. Kleinpoppen, R. Schuch, and H. O. Lutz, J. Phys. B **16**, 1417 (1983).

[8]F. Rösel, D. Trautmann, and G. Baur, Z. Phys. A **304**, 75 (1982).

[9]W. Jitschin, A. Kaschuba, H. Kleinpoppen, and H. O. Lutz, Z. Phys. A **304**, 69 (1982).

[10]E. Horsdal-Pedersen, S. J. Czuchlewski, M. D. Brown, L. D.

Ellsworth, and J. R. Macdonald, Phys. Rev. A **11**, 1267 (1975).
[11]D. L. Matthews, in *Methods of Experimental Physics,* edited by P. Richard (Academic, New York, 1980), Vol. 17, p. 433.
[12]M. O. Krause, J. Phys. Chem. Ref. Data **8**, 307 (1979).
[13]M. H. Chen, B. Crasemann, K. R. Karim, and H. Mark, Phys. Rev. A **24**, 1845 (1981).
[14]C. P. Bhalla, J. Phys. B **8**, 2792 (1975).
[15]J. Hall, P. Richard, T. J. Gray, J. Newcomb, P. Pepmiller, C. D. Lin, K. Jones, B. Johnson, and D. Gregory, Phys. Rev. A **28**, 99 (1983).
[16]G. Basbas, W. Brandt, and R. Laubert, Phys. Rev. A **17**, 1655 (1978).
[17]R. L. Kauffman, J. H. McGuire, P. Richard, and C. F. Moore, Phys. Rev. A **8**, 1233 (1973).
[18]F. Hopkins, R. Brenn, A. R. Whittemore, N. Cue, and V. Dutkiewicz, Phys. Rev. A **11**, 1482 (1975).
[19]T. J. Gray, P. Richard, R. L. Kauffman, T. C. Holloway, R. K. Gardner, G. M. Light, and J. Guertin, Phys. Rev. A **13**, 1344 (1976).
[20]G. Bissinger, P. H. Nettles, S. M. Shafroth, and A. W. Waltner, Phys. Rev. A **10**, 1932 (1974).
[21]R. Anholt, Phys. Rev. A **17**, 983 (1978).
[22]T. Bădică, C. Ciortea, A. Petrovici, I. Popescu, and B. P. Osipenko, X-ray Spectrom. **12**, 173 (1983).
[23]N. Bohr, K. Dan. Vidensk. Selsk. Mat. Fys. Medd. **43**, No. 8 (1948).
[24]H. Schmidt-Böcking, R. Schulé, K. E. Stiebing, K. Bethge, I. Tserruya, and H. Zekl, J. Phys. B **10**, 2663 (1977).
[25]J. U. Andersen, E. Laegsgaard, M. Lund, and C. D. Moak, Nucl. Instrum. Methods **132**, 507 (1976).
[26]E. Morenzoni, R. Anholt, S. Andriamonje, and W. E. Meyerhof, Phys. Rev. A **29**, 2440 (1984).
[27]F. Rösel, D. Trautmann, and G. Baur, Nucl. Instrum. Methods **192**, 79 (1982), and references to earlier work given there.
[28]J. U. Andersen, E. Laegsgaard, and M. Lund, Nucl. Instrum. Methods **192**, 79 (1982).
[29]J. Bang and J. M. Hansteen, K. Dan. Vidensk. Selsk. Mat. Fys. Medd. **31**, No. 13 (1959).
[30]K. E. Stiebing, I. Tserruya, K. Bethge, and H. Schmidt-Böcking, Phys. Lett. **87A**, 24 (1981).
[31]J. Reinhardt, B. Müller, W. Greiner, and G. Soff, Phys. Rev. Lett. **43**, 1307 (1979); G. Mehler, T. de Reus, U. Müller, J. Reinhardt, B. Müller, W. Greiner, and G. Soff (unpublished).